Journal of Photochemistry and Photobiology A: Chemistry 213 (2010) 114–122

Contents lists available at ScienceDirect

Journal of Photochemistry and Photobiology A: Chemistry

journal homepage: www.elsevier.com/locate/jphotochem

IR laser-induced ablation of Ag in dielectric breakdown of gaseous hydrocarbons: Simultaneous occurrence of metastable hcp and stable fcc Ag nanostructures in C:H shell

M. Urbanová [a], D. Pokorná [a], S. Bakardjieva [b], J. Šubrt [b], Z. Bastl [c], P. Bezdička [c], J. Pola [a,*]

[a] Laboratory of Laser Chemistry, Institute of Chemical Process Fundamentals, ASCR, Rozvojova Str. 135, 16502 Prague, Czech Republic
[b] Institute of Inorganic Chemistry, ASCR, 25068 Řež, Czech Republic
[c] J.Heyrovský Institute of Physical Chemistry, ASCR, 18223 Prague, Czech Republic

ARTICLE INFO

Article history:
Received 23 March 2010
Received in revised form 9 May 2010
Accepted 12 May 2010
Available online 20 May 2010

Keywords:
IR laser
Ablation
Dielectric breakdown
Hydrocarbon decomposition
Gas-phase deposition
Nanosized Ag
a-C:H film

ABSTRACT

IR laser-irradiation of Ag in gaseous benzene or ethyne (1 T) results in ablation of Ag target and adjacent dielectric breakdown in gaseous hydrocarbons, the latter leading to dehydrogenation and carbonization reactions in the gas-phase and chemical vapor deposition on both substrate and target of Ag nanoparticles-containing carbonaceous films. The same irradiation of Ag in the hydrocarbons at 50 T induces only dielectric breakdown in the hydrocarbon and leads to gas-phase deposition of carbonaceous films. Volatile products of these processes were examined by FTIR spectroscopy and GC and GC/MS techniques and solid products were characterized by X-ray diffraction, FTIR, X-ray photoelectron and Raman spectroscopy and electron microscopy. These studies revealed co-existence of stable face-centered cubic and metastable hexagonal close-packed Ag-nanophases enveloped by a graphite-like shell and immersed in an amorphous hydrogenated carbon environment having both sp^2- and sp^3-hybridized structures. The nanosized Ag objects show stacking faults and undergo some oxidation in atmosphere to AgO and Ag_3O_4.

1. Introduction

There is a great current interest in synthesis and properties of composite Ag/C films which keep promise for various applications such as optical filters, catalysts, photographic processes and antimicrobial coatings. The methods of fabrication of these films include Ar ion-beam co-sputtering of a silver-graphite target [1,2], simultaneous evaporation of Ag and plasma decomposition/polymerization of chlorobenzene [3], benzene or butane in Ar [4,5], and simultaneous magnetron sputtering of Ag and plasma decomposition/polymerization of methane [6], propane [7] and hexane [8–11] in Ar. The former approach [1,2] results in deposition of Ag nanoparticles encapsulated in amorphous and graphitic carbon matrix, while the latter approaches [3–11] allow deposition of nanostructured Ag/C:H films with Ag nanoparticles embedded in amorphous H-containing diamond-like carbon.

We have recently reported that pulsed IR laser irradiation of some metals in gaseous hydrocarbon (benzene or ethyne, 0.5–50 T) results in gas-phase deposition of metal/carbon films and explained this deposition by concurrent metal ablation and dielectric breakdown in gaseous hydrocarbons [12,13]. The deposition represents a novel laser-assisted approach to metal/carbon nanocomposites and is enabled by ablative incorporation of cobalt or nickel nanoparticles into the gas-phase depositing carbonizing agglomerates.

It was of our further interest to induce laser ablation and dielectric breakdown of hydrocarbon adjacent to silver target. Similar conditions for deposition of Ag/C composite films have been earlier achieved in evaporation/reactive glow-discharge sputtering of Ag in hydrocarbon plasma [3–11]. In both procedures, the Ag target is exposed to plasma-produced carbonaceous products formed from hydrocarbon decomposition and the proceeding interaction of plasma with target leads to deposition on both substrate and target and inevitably involves interaction with carbon-coated silver. Having considered that deposition on neighboring target and distant substrate may produce structurally different products, we thought rational to examine the process of pulsed IR laser-induced plasma decomposition of benzene and ethyne adjacent to silver target and compare spectral properties and morphology of solid films deposited on surfaces of target and substrate.

2. Experimental

IR-laser irradiation experiments were conducted in a Pyrex reactor (70 mL in volume) in vacuum or in the presence of gaseous ethyne or benzene at pressures of 1 and 50 T. The samples of the hydrocarbons were irradiated by a pulsed TEA CO_2 laser (model

* Corresponding author. Tel.: +420 220390308; fax: +420 220920661.
E-mail address: pola@icpf.cas.cz (J. Pola).

1010-6030/$ – see front matter © 2010 Elsevier B.V. All rights reserved.
doi:10.1016/j.jphotochem.2010.05.009

1300 M, Plovdiv University) operating with a frequency of 1 Hz on the P(20) line of the $00^01–10^00$ transition (944.19 cm^{-1}) and a pulse energy of 1.8 J. This radiation was focused with a NaCl lens (f. l. 15 cm) on an Ag target positioned in the center of the reactor above which was accommodated a copper substrate. The pulsed irradiation of Ag at 1 T, resulting in Ag ablation and decomposition of the hydrocarbon, allowed deposition of little adherent Ag/C films on the Cu substrate and adherent Ag/C layers on the irradiated target. The irradiation at 50 T did not lead to Ag ablation and allowed deposition of only carbonaceous films.

The reactor was described elsewhere [13] and it was a tube fitted at each end with KBr windows and having a port with rubber septum enabling GC and GC/MS analyses of gaseous content and a PTFE valve connecting to vacuum manifold and pressure transducer.

The progress of ethyne and benzene decomposition and volatile decomposition products were analyzed directly in the reactor by FTIR spectrometry (an FTIR Nicolet Impact spectrometer, resolution 4 cm^{-1}) using diagnostic absorption bands of benzene at 1037 cm^{-1} and ethyne at 3268 cm^{-1}. Aliquots of the irradiated reactor content were sampled by a gas-tight syringe and analyzed by gas chromatography-mass spectroscopy (a Shimadzu QP 5050 mass spectrometer, 50-m Porabond capillary column, programmed temperature 30–200 °C). The decomposition products were identified through their FTIR spectral diagnostic bands (C_2H_2, 731 cm^{-1}; C_4H_2, 628 cm^{-1}; CH_4, 1305 and 3016 cm^{-1}) and through their mass spectra using the NIST library.

The deposited films were analyzed with the FTIR Nicolet Impact spectrometer, a Nicolet Almega XR Raman spectrometer (resolution 2 cm^{-1}, excitation wavelength 473 nm and power 10 mW) and by electron microscopy (a Philips XL30 CP scanning electron microscope equipped with an energy-dispersive analyzer EDAX DX-4 of X-ray radiation) and a JEOL JEM 3010 microscope operating at 300 kV and equipped with an EDS detector (INCA/Oxford) and CCD Gatan (Digital Micrograph software). The transmission electron analysis was carried out on ground samples that were subsequently dispersed in ethanol followed by application of a drop of a diluted suspension on a Ni grid. The EDX and SAED-determined atomic percentage of C, O and Ag elements correspond to 5% error.

Diffraction patterns were measured with a PANalytical X'Pert PRO diffractometer equipped with a conventional X-ray tube (Co-Kα radiation, 40 kV, 30 mA, point focus), an X-ray monocapillary with diameter of 0.1 mm, and a multichannel detector X'Celerator with an anti-scatter shield.

The C 1s, O 1s and Ag $3d_{5/2}$ photoelectron spectra and C KLL Auger spectra of the deposited films were measured in an ESCA 310 (Scienta) electron spectrometer with a base pressure better than 10^{-9} T using Al-Kα radiation (1486.6 eV) for electron excitation. The surface composition of the deposited film was determined by correcting the spectral intensities for subshell photoionization cross-sections [14].

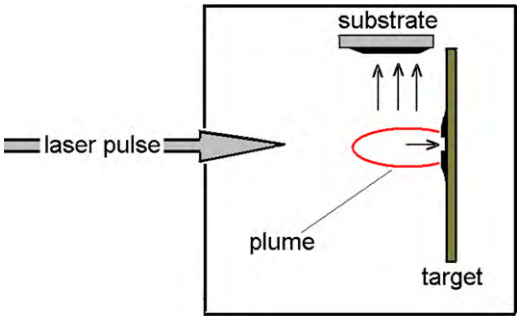

Fig. 1. Scheme of gas-phase deposition.

Benzene (Lachema, purity better than 99.7%) and ethyne (Linde, purity better than 98.5%) were evaporated from the liquid nitrogen-solidified compounds on a vacuum line prior to use.

3. Results and discussion

3.1. IR laser irradiation of Ag in gaseous hydrocarbons

The TEA CO_2 laser irradiation of Ag target in the presence of gaseous benzene or ethyne (1 or 50 T) is accompanied with a visible luminescence and results in the decomposition of the hydrocarbons and a significant deposition of black Ag/C films on the Cu substrate (and the nearby reactor surface) and a minute deposition on the irradiated target (Fig. 1).

The repetitive laser pulses lead to accumulation of the mass of products of Ag ablation and hydrocarbon dielectric breakdown mainly on the substrate (and nearby reactor surface). A small part of these products is also deposited on the surface of the Ag target, but a fraction of this deposit is repeatedly removed by next pulses. This brings about a steady growth of the film deposited on the Cu substrate and the deposition of much thinner films, having an uncovered region in the incident area (ca. mm^2) of the pulse, on the Ag target.

The irradiations conditions used were identical to those of laser irradiation of Co and Ni in benzene, which were proved by optical emission spectra to yield metal atoms and ions (Co and Ni plasma, arising from the laser ablation) together with H atoms and neutral and cationic carbon species (arising from the dielectric breakdown in the hydrocarbon [12]).

The depletion of ethyne and benzene at 1 T but not at 50 T is affected by the nature of the hydrocarbon. The more efficient depletion of benzene than that of ethyne at 1 T and the same depletion rate of benzene and ethyne at 50 T (Fig. 2) are in agreement with our earlier observations [13] and presumption that more efficient decomposition of benzene takes place in a significant Ag plasma and that comparable decomposition of benzene and ethyne occurs mostly in dielectric breakdown when Ag ablation is small. The dif-

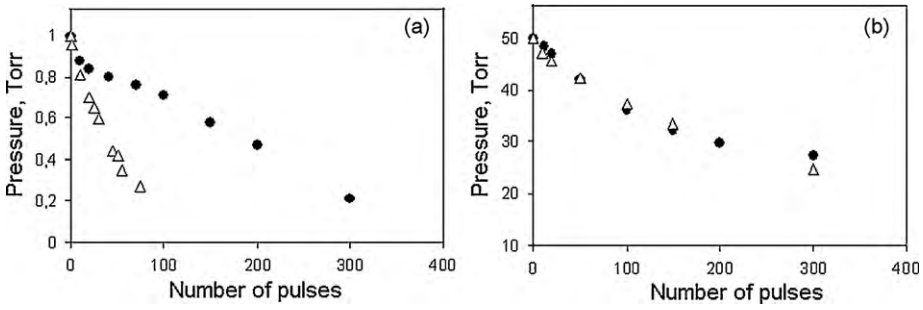

Fig. 2. Hydrocarbon (Δ, benzene; ●, ethyne) depletion as dependent on number of laser pulses at initial pressure 1 T (a) and 50 T (b).

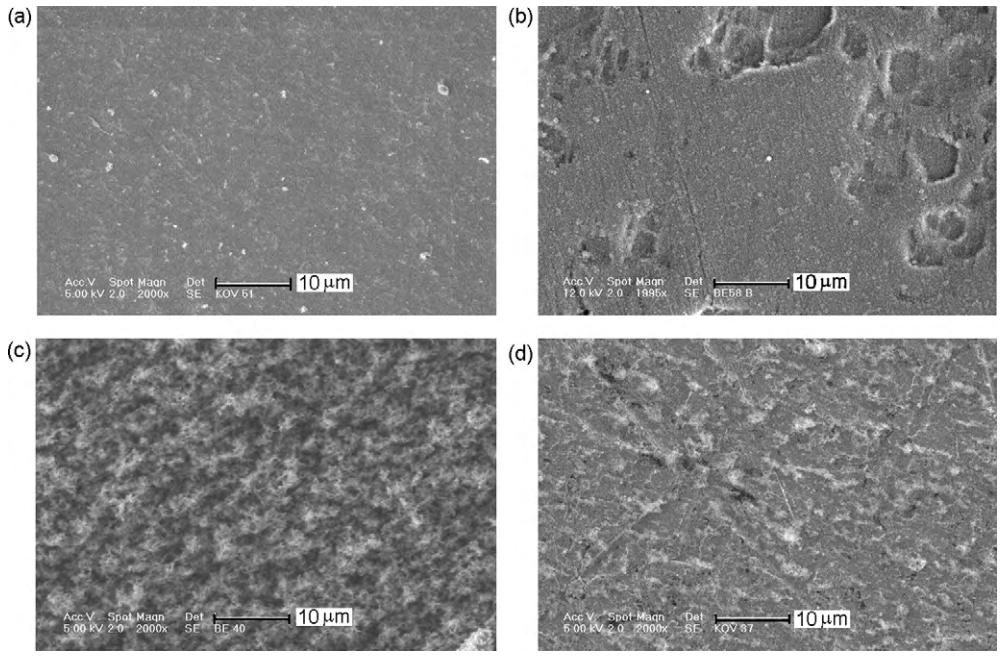

Fig. 3. SEM images of films deposited on Cu substrate from 1 T of ethyne (a), 1 T of benzene (b), 50 T of benzene (c) and 50 T of ethyne (d).

ferent decomposition capability of benzene and ethyne is in line with Ag-surface-assisted C–H and C–C bond cleavages in these compounds [15–17]. The catalytic effect of Ag in similar reactions has been reported only for hydroarylation of olefins with arenes by Pt–Ag complexes [18]. The catalytic effect of Ag nanostructures is also known for very different reactions as e.g. reduction of dyes [19] or nitroarenes [20]. Similarly to Co and Ni plasma-containing metal atoms and cations [12] the Ag plasma may involve neutral and cationic species; unequivocal evidence on catalytic effect of these particular species can come from discriminating some of these species at conditions allowing selective formation.

The gaseous decomposition products of benzene and ethyne differ, but the product composition for each hydrocarbon is virtually independent of the initial pressure and the decomposition progress. Benzene is decomposed to ethyne (~60 mole%), ethene (~20–25 mole%), butadiyne (~10 mole%) and propane, 1-buten-3-yne, C_3H_4, and ethynylbenzene (each 0.1–0.6 mole%), whereas ethyne yields butadiyne as a major product (90–95 mole%) and C_3H_4 and 1,3-butadiene (each 2–4 mole%) as minor products. These products and the carbonaceous solid deposit show that benzene and ethyne undergo decomposition and dehydrogenation steps typical for their thermal carbonization [15–17].

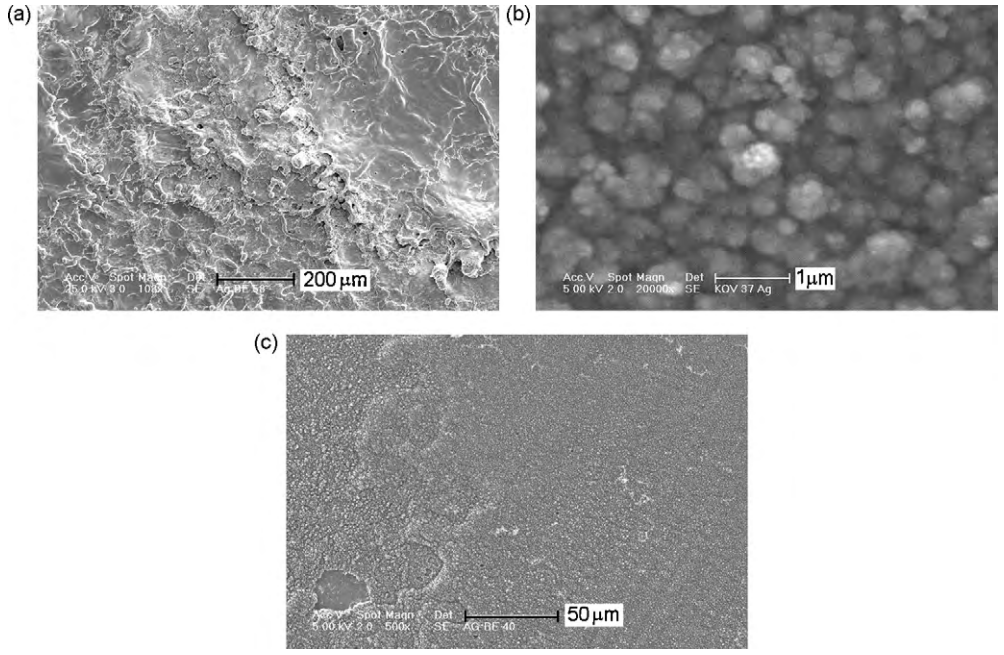

Fig. 4. SEM images of Ag target ablated in vacuum (a) and of films deposited on Ag target from 50 T of ethyne (b) and 50 T of benzene (c).

Table 1
Atomic% of Ag in carbonaceous deposit on Cu substrate and Ag target.

Hydrocarbon	Pressure, T	Decomposition progress, %	Ag atomic% on Cu substrate	Ag atomic% on Ag target
Benzene	1[a]	78	2.0	25
	50[b]	50	0	0
Ethyne	1[b]	30	0.4	57
	50[b]	46	0	16

[a] 100 pulses.
[b] 300 pulses.

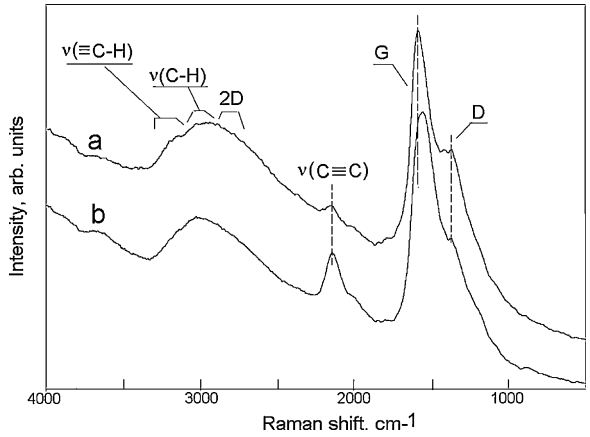

Fig. 5. Raman spectra of film deposited on Cu from 50 T of benzene (a) and ethyne (b).

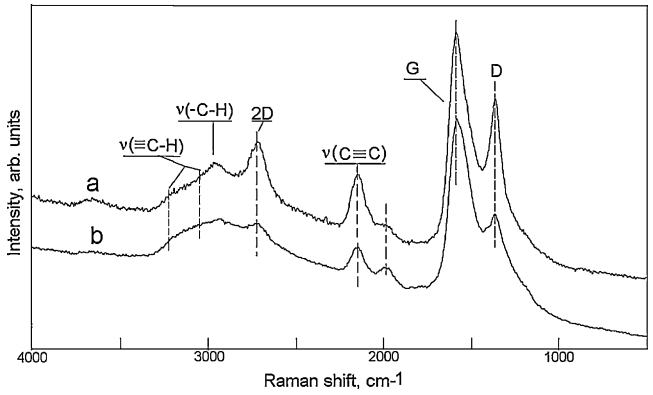

Fig. 6. Raman spectra of films on Ag target from 50 T of ethyne. (The μm^2 areas were measured near the crater (a) and 1–3 mm afar (b).)

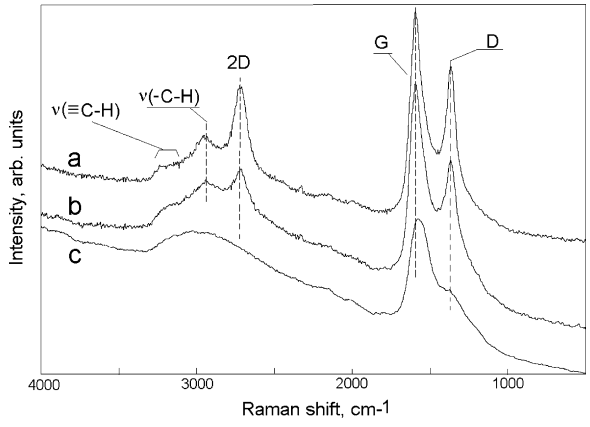

Fig. 7. Raman spectra of films on Ag target from 1 T of ethyne. (The μm^2 areas were measured near the crater (a) and 1 mm (b) and 3 mm (c) afar.)

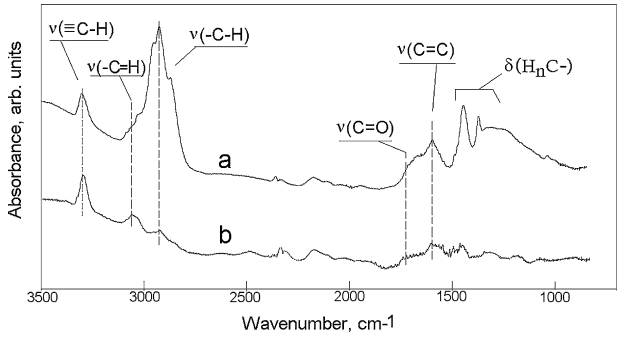

Fig. 8. ATR FTIR spectra of films deposited on Ag target (a) and Cu substrate (b) from 50 T of benzene.

3.2. Properties of deposited Ag/C films

The black solid films were deposited from benzene and ethyne on the Cu substrate and to a lesser extent on the irradiated target with typically 100 pulses (for 1 T of hydrocarbon) and 300 pulses (for 50 T of hydrocarbon). They were analyzed for their morphology and spectral properties and revealed to possess features depending on the deposition site.

The SEM–EDX analysis of the films deposited on the Cu substrate at 1 T shows the prevalence of carbon, traces of oxygen (less than 1–3 atomic% of carbon) and low amounts of Ag, whereas that of the films deposited on Cu at 50 T reveals only carbon (and traces of oxygen; Table 1). This indicates that the Ag plasma (ablation) is, similarly to Co and Ni ablation [12], more significant at the lower hydrocarbon pressure. The SEM–EDX analysis of the films deposited on the Ag target shows large amounts of carbon and Ag; we assume that these films are much thinner than those deposited on Cu and that the determined amount of Ag reflects both ablated and non-ablated mass.

The SEM images of the films deposited on the Cu substrate at 1 and 50 T of hydrocarbon show different morphology. The films deposited at 1 T are smooth and without defects (deposition from

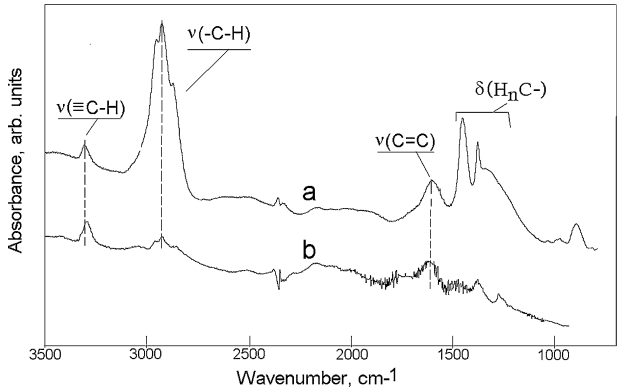

Fig. 9. ATR FTIR spectra of films deposited on Ag target (a) and Cu substrate (b) from 50 T of ethyne.

ethyne, Fig. 3a) or have several μm-sized valleys (deposition from benzene, Fig. 3b). The films deposited at 50 T reveal fluffy structures that are more copious when obtained from benzene than from ethyne (Fig. 3c and d).

The SEM images of the Ag target ablated in vacuum (Fig. 4a) show several up to several tens μm-sized round-shaped bodies extending from the surface; this morphology can be considered as a primary stage of an ensuing separation of these bodies leading to ablation. The images of the films deposited on the target from 1 or 50 T of benzene and ethyne are virtually identical and we give, for the sake of simplicity, only images of the target irradiated at 50 T at different magnification. It is seen (Fig. 4b and c) that the Ag target is covered with a film composed of somewhat rough and less than 1 μm-sized round-shaped and loosely attached Ag-rich C/Ag composite particles (Fig. 4b) that come out at lower magnification (Fig. 4c) as almost smooth layers having several μm-sized valleys.

More information on the nature of the deposited films is obtained from the visible Raman spectra which depend on whether the films are deposited on the Ag target or the Cu substrate (Figs. 5–7). The spectra of the films deposited on Cu at 1 and 50 T (Fig. 5) are very similar and we illustrate them in Fig. 5. They are dominated by G and D bands of unsaturated sp^2 carbon and possess second-order (overtone and combination) bands and bands assignable to C–H and C≡C stretches [21–24]. The G band is centered at 1560–1590 cm^{-1}, a broad band between 2630 and 3280 cm^{-1} corresponds to the 2D band and stretching vibrations of the C(sp–sp^3)–H bonds, a medium and low-intensity band at 2150 cm^{-1} relates to stretching vibration of the triple bond, and a low-intensity band at 1370 cm^{-1} (with benzene) or a bifurcated shoulder at 1410 and 1370 cm^{-1} (with ethyne) correspond to the D band of carbon. The spectra obtained from ethyne have a higher content of the C≡C bond.

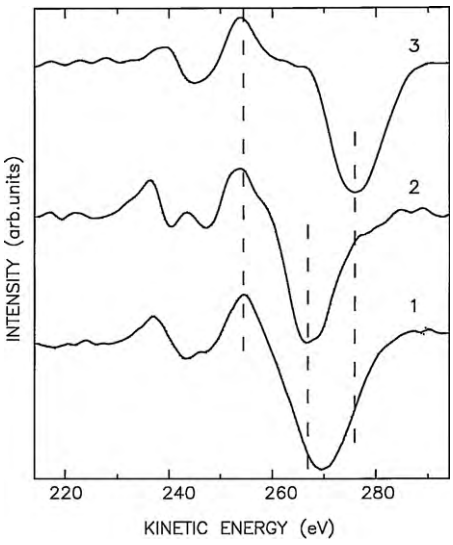

Fig. 10. Derivative Auger C KLL spectrum of the deposited film on Ag (1). For the purpose of comparison the spectra of diamond (2) and graphite (3) are also included.

The spectra of the films deposited on the Ag target at 50 T do not virtually differ and we show, for the sake of brevity, only those deposited from ethyne. These were measured (Fig. 6) at different positions from the impinging laser pulses (crater). The more separated D, G and 2D bands, along with a more intense ν(C≡C) band, are observed for the area near the crater. The former are compatible with a more organized C(sp^2) (graphitic) form of carbonaceous deposit in this location.

The spectra of films deposited on the Ag target from 1 T do not differ for ethyne and benzene and an illustration revealing their

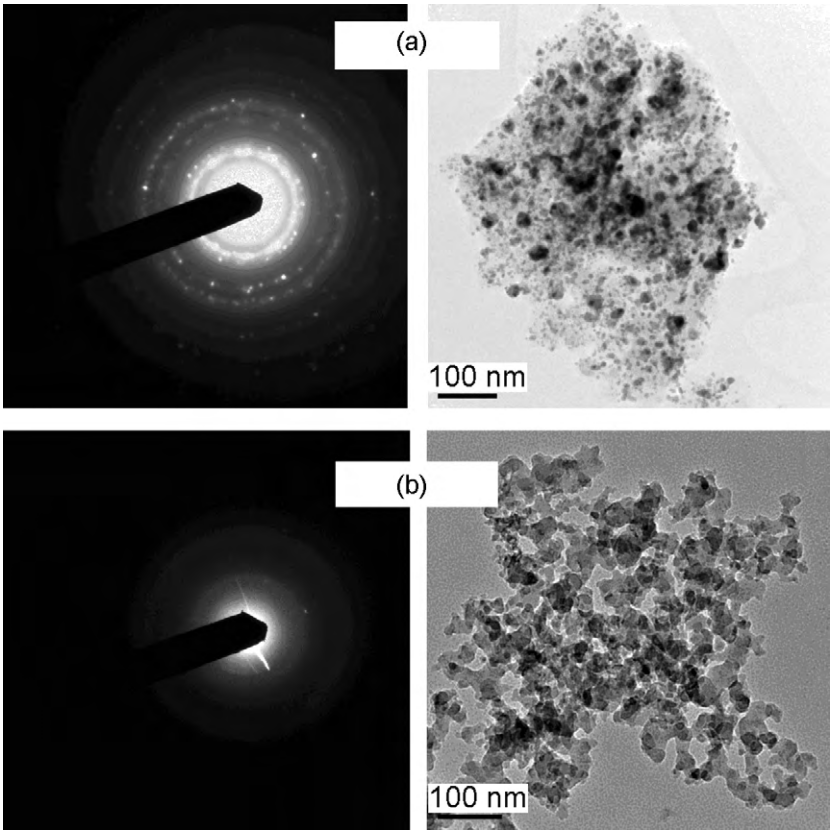

Fig. 11. Electron diffraction and TEM images of films deposited on Cu substrate from 1 T (a) and 50 T (b) of benzene.

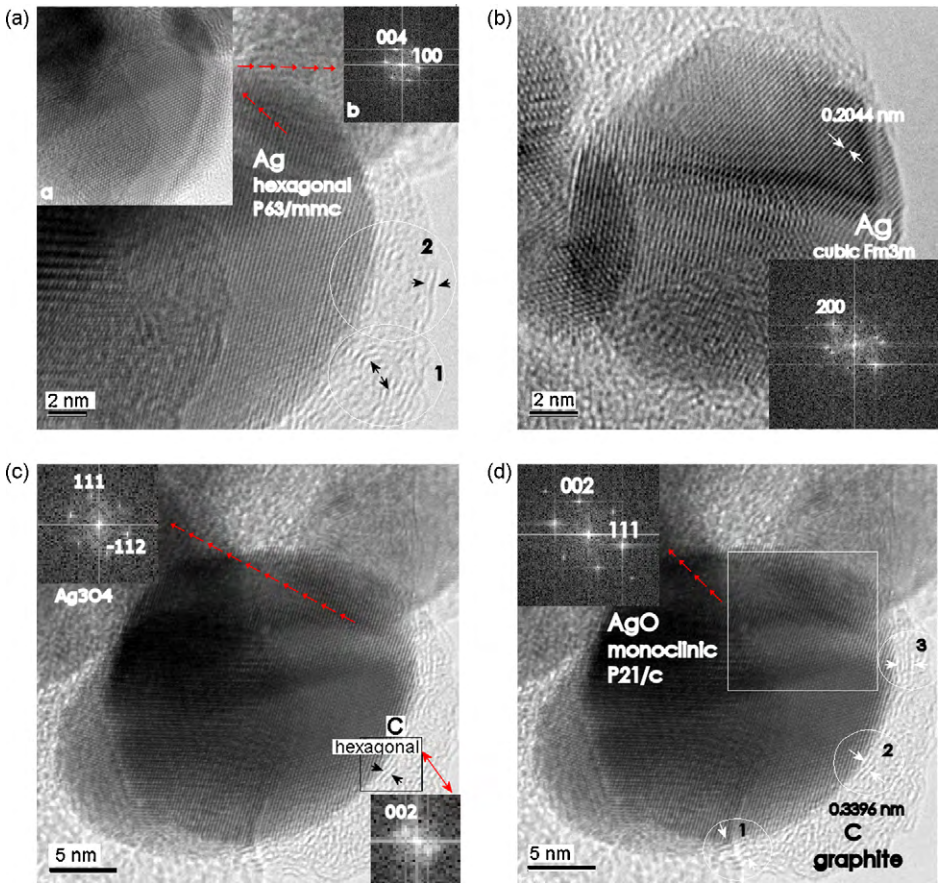

Fig. 12. HRTEM images of films deposited on Cu substrate from 1 T of benzene. The identified nanobjects of hexagonal Ag (a), cubic Ag (b), Ag_3O_4 (c) and AgO (d) are enveloped with regions of hexagonal graphitic carbon (indexed by numbers 1–3).

dependence on the measured position is given only for films from ethyne (Fig. 7). The absence of the ν(C≡C) band is in accordance with a simpler carbon structure and the observed decrease in the D/G band ratio with increasing distance from the crater reflects more graphitization in the area close to the crater.

We note that the G band reflects bond stretches of all pairs of sp^2 atoms in rings and chains and that the D band relates to breathing modes of rings (e.g. [24,25]). The positions of the G and D bands resemble those of graphitic a-C:H films and soot [21,23,25]. It is known that the G peak position varies from 1520 cm^{-1} for amorphous carbons to 1590 cm^{-1} for glassy carbons [26] and that it fits higher values in this range for films with low sp^3 content [27]. The films deposited near the Ag crater can therefore be deduced to have more pronounced graphitic features due to more cyclic sp^2 structures.

The ATR FTIR spectra of the films deposited on the Ag target and the Cu substrate at 50 T (Figs. 8 and 9) show bands at 3295–3304, 2930, 1600–1620 and 1450–1375 cm^{-1} that are, in the given order, assigned [28] to ν(≡C–H), $\nu(C^{sp3}$–H), ν(C=C) and $\delta(H_nC$–) vibrations. The shoulder at 1710 cm^{-1} and the band at 1375 cm^{-1} respectively correspond to the (ν(C=O) and ν(OCO) carbonyl stretches and are accounted for by a minor oxidation at the C=C bonds. The more intense $\nu(C^{sp3}$–H) bands at 2930 cm^{-1} observed on Ag target are indicative of cross-linking of C=C bonds leading to saturated carbon moieties and may also be due to Ag-surface-enhanced vibrations [10].

The XPS analysis-derived stoichiometry of the films deposited on the Ag target at 1 T – $C_{1.00}Ag_{0.04}O_{0.13}$ – is indicative of the presence of Ag and O in the topmost layers. While the O content is commonly attributed to superficial oxidation of sp^2 carbon in atmosphere, the Ag content is ascribed to Ag nanoparticles [29,30] dispersed in the carbon film, because the binding energy of Ag $3d_{5/2}$ electrons 368.7 eV is by 0.4 eV higher than that of bulk Ag.

The X-ray excited Auger C KLL derivative spectrum of the deposit, allowing to estimate the sp^3/sp^2 hybridization ratio [28–30] is compared to those of graphite and diamond in Fig. 10. The separation between the most positive and the most negative minimum, 15.4 eV, used to estimate sp^3/sp^2 [31–33] ratio corresponds neither to sp^2 nor sp^3 hybridization but rather to the presence of 40% of sp^2-hybridized carbon in superficial layers of the deposit.

The X-ray diffraction of all films reveals no crystalline form of Ag or C and it shows only the fcc-crystalline phase of the Cu substrate (syn-Cu). This is in line with thin amorphous structure.

The electron diffraction confirms polycrystalline nature of films deposited at 1 T and fully amorphous phase of films deposited on Cu at 50 T (Fig. 11). The concentric spots observed in films deposited at 1 T indicate the presence of nanocrystals and the TEM images reveal nanostructured character of the amorphous phase and chain-like nanostructures (Fig. 11).

The selective area ED (electron diffraction) analysis of the films deposited from 1 T ($C_{1.00}Ag_{0.10}$) shows a low content of Ag in the carbon environment, which is in line with the EDX–SEM-derived analysis. The HRTEM (high-resolution transmission electron microscopy) images reveal nanoparticles of hexagonal and cubic silver and nanoforms of silver oxides (AgO and Ag_3O_4 enveloped by a carbon shell (Fig. 12) whose morphology pattern was earlier recognized [34,35] to consist of rather concentric and curved arrangements of graphene layers.

This form of carbon is considered [36] to be a primary stage of carbon graphitization and has been found in all films deposited

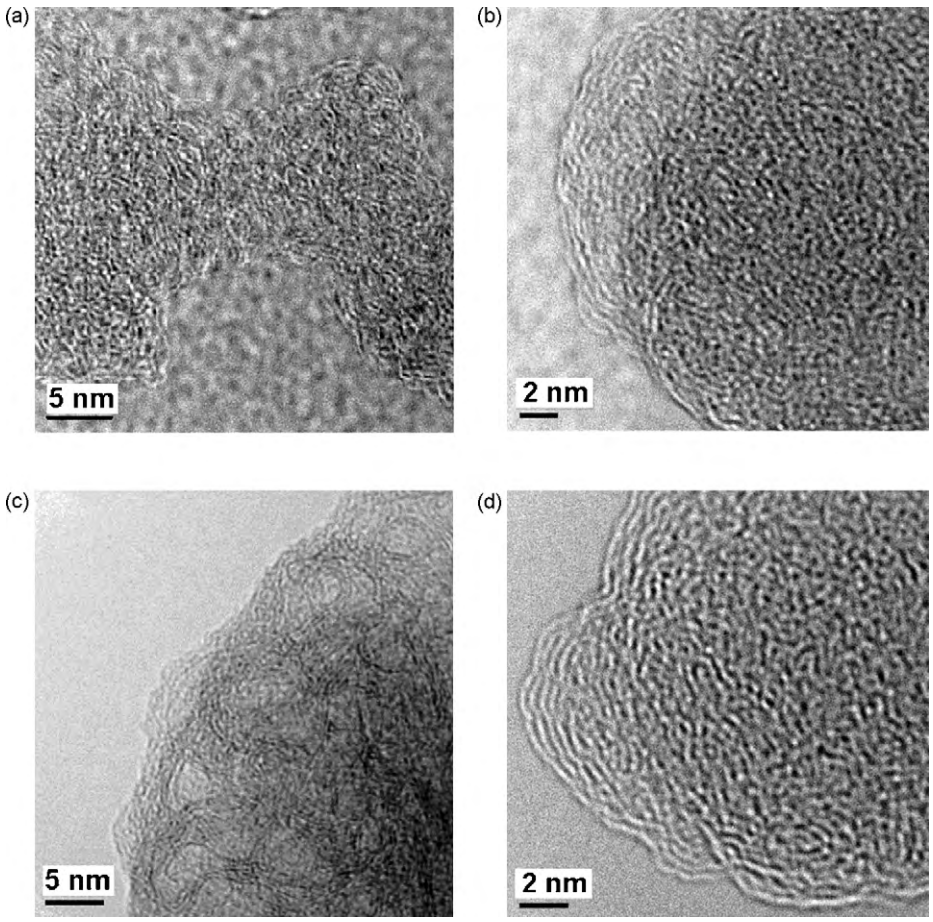

Fig. 13. Curved and concentric carbon layers in HRTEM images of films deposited on Cu substrate from 1 T of ethyne (a), 1 T of benzene (b), 50 T of benzene (c) and 50 T of ethyne (d).

at 1 T (e.g. Fig. 11) and 50 T (e.g. Fig. 12). Better illustration is provided in Fig. 13 showing three different patterns of these morphologies.

We note that that the face-centered cubic (fcc) Ag phase is quite common, whereas the hexagonal close-packed (hcp) structure of Ag is rare and has been found only in mineral deposits from northeastern Russia [37] and recently identified in silver nanoparticles [38], epitaxially grown films [39] and Ag nanoobjects grown in small-pore alumina membranes [40–42]. The metastable hcp nanophases preferably grow in nanosized pores of membranes and can become deformed by electron beam and give rise to fcc-crystalline particles with stacking faults and twin boundaries [41]. Plenty of HRTEM images of films deposited at 1 T have regions of these defects (e.g. Fig. 14) and prove that both hcp and fcc structures co-exist as closely attached nanoobjects.

The pulsed irradiation causes the Ag ablation and hydrocarbon decomposition/carbonization within the order of μs and we presume that the observed feasible deposition of the Ag metastable structures is due to fast heating (ablation and dielectric breakdown) and in particular due to fast cooling of the depositing products. This assumption is supported by observation of metastable nanoalloys of Si, Ge and Sn deposited from the pulsed IR laser irradiation of binary mixtures of silane, germane and stannane (e.g. [43–45]).

The observed nanoforms of Ag oxides, i.e. AgO and Ag_3O_4, can be only explained by oxidation of Ag nanoparticles in atmosphere. The oxide nanoforms are thermodynamically less stable than Ag_2O [46] that has not been detected in our experiments. We assume that the AgO and Ag_2O_3 are formed by reaction of incompletely carbon-enveloped Ag nanoparticals with air. The relatively high BET surface of the carbonaceous deposit and significant interaction of laser-deposited carbonaceous powders with $^3O_2$ [47,48] suggest that this oxidation is facilitated by diffusion.

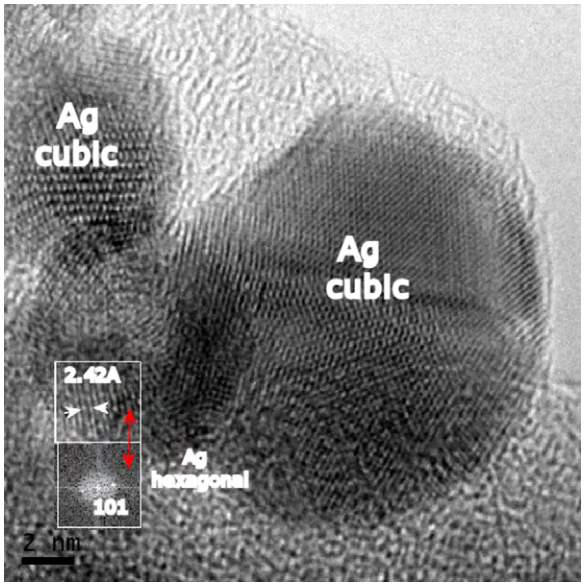

Fig. 14. HRTEM image of film deposited on Cu from 1 T of benzene illustrating nanoobject of metastable hcp Ag fixed between two stable fcc Ag-nanophases.

4. Conclusions

The pulsed IR laser irradiation of Ag in 1 T of gaseous benzene and ethyne leads to ablation of Ag and adjacent dielectric-breakdown-induced decomposition of the hydrocarbons. Both processes allow chemical vapor deposition of Ag nanoparticles-containing carbonaceous films.

The same irradiation of Ag in 50 T does not lead to Ag ablation and results in dielectric breakdown-induced of hydrocarbons, affording deposition of carbonaceous films.

The volatile products of the hydrocarbon decomposition are typical for thermal decomposition of these compounds and indicate dehydrogenation, C–C bond cleavages and radical combinations resulting in H-poor carbonaceous species that combine to amorphous hydrogenated ultrafine carbon soot.

The Ag-containing and non-containing carbonaceous films have different structure when deposited on distant substrate and nearby Ag target. More organized carbon structure with higher Csp^2 content and more graphitic features were deposited at Ag target and on position close to the impinging laser pulse (crater).

The Ag nanoparticles are a blend of stable face-centered cubic and metastable hexagonal close-packed Ag-nanophases and are recognized as enveloped by a graphite-like shell and immersed in an amorphous hydrogenated carbon environment having both sp^2 and sp^3-hybridized structures.

The nanosized Ag objects show stacking faults and undergo some oxidation in atmosphere to AgO and Ag_3O_4.

The reported procedure of chemical vapor deposition of the hcp-nanoforms of Ag is one of few processes leading to formation of this rare structure.

Acknowledgements

The authors thank the Ministry of Education, Youth and Sports of the Czech Republic (grant no. LC523) and the Czech Science Foundation (GAAVCR grant no. 400720619) for funding this research.

References

[1] D. Babonneau, T. Cabioc'h, A. Naudon, J.C. Girard, M.F. Denanot, Silver nanoparticles encapsulated in carbon cages obtained by co-sputtering of the metal and graphite, Surf. Sci. 409 (1998) 358–371.
[2] D. Babonneau, A. Naudon, D. Thiaudière, S. Lequien, Morphological characterization of ion-sputtered C–Ag, C/C–Ag and Ag/C films by GISAXS, J. Appl. Crystallogr. 32 (1999) 226–233.
[3] G. Kampfrath, A. Heilmann, C. Hamann, Plasma polymerized thin films containing small silver particles, Vacuum 38 (1988) 1–3.
[4] H. Biederman, I. Chudáček, D. Slavinská, L. Martinů, J. David, S. Nešpůrek, Physical properties of metal/a-C:H composite films, Vacuum 39 (1989) 13–15.
[5] H. Biederman, Z. Chmel, A. Fejfar, M. Mišina, J. Pešička, Temperature induced structural rearrangements of Ag/a-C:H composite films and their dc electrical conduction, Vacuum 40 (1990) 377–380.
[6] J.T. Harnack, C. Benndorf, The deposition of Ag–C:H films: a tool to understand the role of carbide-forming metals in the Me–C:H deposition process, Mater. Sci. Eng. A 140 (1991) 764–769.
[7] H. Biederman, K. Kohoutek, Z. Chmel, V. Stary, R.P. Howson, Hard carbon and composite metal hard carbon films prepared by a dc unbalanced planar magnetron, Vacuum 40 (1990) 251–255.
[8] H. Biederman, P. Hlídek, J. Pešička, D. Slavinská, V. Stundžia, Deposition of composite metal/C:H films—the basic properties of Ag/C:H, Vacuum 47 (1996) 1385–1388.
[9] H. Biederman, R.P. Howson, S. Slavinská, V. Stundžia, J. Zemek, Composite metal/C:H films prepared in an unbalanced magnetron, Vacuum 48 (1997) 883–886.
[10] H. Boldyryeva, P. Hlídek, H. Biederman, D. Slavinská, A. Choukourov, Composite Ag/C:H films prepared by DC planar magnetron deposition, Thin Solid Films 442 (2003) 86–92.
[11] J. Hanus, M. Drabík, P. Hlídek, H. Biederman, G. Radnoczi, D. Slavinská, Some remarks on Ag/C:H nanocomposite films, Vacuum 83 (2009) 454–456.
[12] M. Santos, L. Díaz, J.J. Camacho, M. Urbanová, D. Pokorná, J. Šubrt, S. Bakardjieva, Z. Bastl, J. Pola, IR laser-induced metal ablation and dielectric breakdown in benzene, Infrared Phys. Technol. 53 (2010) 23–28.
[13] J. Pola, M. Urbanová, D. Pokorná, J. Šubrt, S. Bakardjieva, P. Bezdička, Z. Bastl, IR laser-induced formation of amorphous Co–C films with crystalline Co, Co_2C and Co_3C nanograins in a graphitic shell, J. Photochem. Photobiol. A 210 (2010) 153–161.
[14] J.H. Scofield, Hartree-Slater subshell photoionization cross-sections at 1254 and 1487 eV, J. Electron Spectrosc. Relat. Phenom. 8 (1976) 129–137.
[15] J.H. Kiefer, L.J. Mizerka, M.R. Patel, H.-C. Wei, A shock tube investigation of major pathways in the high temperature pyrolysis of benzene, J. Phys. Chem. 89 (1985) 2013–2019.
[16] M.H. Back, Mechanism of the pyrolysis of acetylene, Can. J. Chem. 49 (1971) 2199–2204.
[17] H. Ogura, Pyrolysis of acetylene behind shock waves, Bull. Chem. Soc. Jpn. 50 (1977) 1044–1050.
[18] D. Karshtedt, A. Bell, T.D. Tilley, Pt–Ag catalysts system for hydroarylation with unactivated arenes and olefins, Organometallics 23 (2004) 4169–4171.
[19] Z.-J. Jiang, C.-Y. Lin, L.-W. Sun, Catalytic properties of silver nanoparticles supported on silica spheres, J. Phys. Chem. B 109 (2005) 1730–1735.
[20] M.H. Rashid, T.K. Mandal, Synthesis and catalytic application of nanostructured silver dendrites, J. Phys. Chem. C 111 (2007) 16750–16760.
[21] J. Schwan, S. Ulrich, K. Jung, H. Ehrhardt, R. Samlenski, R. Brenn, Deposition of ta–C:H films by r.f. plasma discharges, Diamond Relat. Mater. 4 (1995) 304–308.
[22] A. Cuesta, P. Dhamelincourt, J. Laureyns, A. Martínez-Alonso, J.M.D. Tascón, Raman microprobe studies on carbon materials, Carbon 32 (1994) 1523–1532.
[23] A.C. Ferrari, J. Robertson, Interpretation of Raman spectra of disordered and amorphous carbon, Phys. Rev. B 61 (2000) 14095–14107.
[24] R.O. Dillon, J.A. Woollam, V. Katkanant, Use of Raman scattering to investigate disorder and crystalline formation in as-deposited and annealed carbon films, Phys. Rev. B 29 (1984) 3482–3489.
[25] P.K. Bachmann, D.U. Wiechert, in: R.E. Clausing, et al. (Eds.), Diamond and Diamond-Like Films and Coatings, Pergamon Press, 1991, p. 677.
[26] M. Yoshikawa, G. Katagiri, A. Ishida, A. Ishitani, Raman spectra of diamondlike amorphous carbon films, Solid State Commun. 66 (1988) 1177–1180.
[27] S. Prawer, K.W. Nugent, Y. Lifshitz, G.D. Lempert, E. Grossman, J. Kulik, I. Avigal, R. Kalish, Systematic variation of the Raman spectra of DLC films as a function of sp^2:sp^3 composition, Diamond Relat. Mater. 5 (1996) 433–438.
[28] R.G.J. Miller, H.A. Willis (Eds.), Infrared Structural Correlation Tables and Data Cards, Heyden & Son Lyd, Spectrum House, London, 1969.
[29] P. Ptáček, Z. Bastl, XPS characterization of supported bimetallic palladium–silver clusters, Appl. Surf. Sci. 45 (1990) 319–323.
[30] R. Dietsche, D.C. Lim, M. Bubek, I. Lopez-Salido, G. Gantefor, Y.D. Kim, Comparison of electronic structures of mass-selected Ag clusters and thermally grown Ag islands on sputter-damaged graphite surfaces, Appl. Phys. A90 (2008) 395–398.
[31] A.A. Galuska, H.H. Madden, R.E. Allred, Electron spectroscopy of graphite, graphite oxide and amorphous carbon, Appl. Surf. Sci. 32 (1988) 253–272.
[32] J.C. Lascovich, R. Giorgi, S. Scaglione, Evaluation of the sp^2/sp^3 ratio in amorphous carbon structure by XPS and XAES, Appl. Surf. Sci. 47 (1991) 17–21.
[33] J. Pola, M. Urbanová, Z. Bastl, Z. Plzák, J. Šubrt, V. Vorlíček, I. Gregora, C. Crowley, R. Taylor, Laser photolysis of liquid benzene and toluene: graphitic and polymeric carbon formation at ambient temperature, Carbon 35 (1997) 605–611.
[34] I. Morjan, I. Voicu, F. Dumitrache, I. Sandu, I. Soare, R. Alexandrescu, E. Vasile, I. Pasuk, R.M.D. Brydson, H. Daniels, B. Rand, Carbon nanopowders from continuous-wave CO_2 laser-induced pyrolysis of ethylene, Carbon 41 (2003) 2913–2921.
[35] N. Herlin, I. Bohn, C. Reynaud, M. Cauchetier, A. Galvez, J.N. Rouzaud, Nanoparticles produced by laser pyrolysis of hydrocarbons: analogy with carbon cosmic dust, Astron. Astrophys. 330 (1998) 1127–1135.
[36] I. Morjan, I. Voicu, R. Alexandrescu, I. Pasuk, I. Sandu, F. Dumitrache, I. Soare, T.C. Fleaca, M. Ploscaeu, V. Ciupina, H. Daniels, A. Westwood, B. Rand, Gas composition in laser pyrolysis of hydrocarbon-based mixtures: Influence on soot morphology, Carbon 42 (2004) 1269–1273.
[37] M.I. Novgorodova, A.I. Gorshkov, A.V. Mokhov, Native silver and its new structural modifications, Zap. Vses. Mineral. Obshch. 108 (1979) 552–563.
[38] P. Taneja, R. Banerjee, R. Ayyub, P. Chandra, G.K. Dey, Observation of a hexagonal (4H) phase in nanocrystalline silver, Phys. Rev. B 64 (2001), 033405–4 pp.
[39] E. Wetli, M. Hochstrasser, M. Erbudak, Epitaxial growth of Ag in the hexagonal structure, Surf. Sci. 377 (1997) 876–881.
[40] B.H. Hong, C.B. Bae, C.W. Lee, S. Yeong, K.S. Kim, Ultrathin single-crystalline silver nanowire arrays formed in an ambient solution phase, Science 294 (2001) 348–351.
[41] C. Liang, K. Terabe, T. Hasegawa, M. Aono, Formation of metastable silver nanowires of hexagonal structure and their structural transformation under electron beam irradiation, Jpn. J. Appl. Phys. 45 (2006) 6046–6048.
[42] X. Liu, J. Luo, J. Zhu, Size effect on the crystal structure of silver nanowires, Nano Lett. 6 (2006) 408–412.
[43] T. Křenek, P. Bezdička, N. Murafa, J. Šubrt, J. Pola, Laser CVD of nanodisperse Ge–Sn alloys obtained by dielectric breakdown of SnH_4/GeH_4 mixtures, Eur. J. Inorg. Chem. (2009) 1464–1467.

[44] T. Křenek, P. Bezdička, N. Murafa, J. Šubrt, P. Duchek, J. Pola, IR Laser-induced CVD of beta-Sn/SnSi-nanodisperse alloys from stannane–silane mixture, J. Anal. Appl. Pyrolysis 86 (2009) 381–385.
[45] T. Křenek, N. Murafa, P. Bezdička, J. Šubrt, J. Pola, IR Laser CVD of nanostructured Si/Ge alloy from silane–germane mixture, J. Anal. Appl. Pyrolysis, submitted for publication.
[46] J.F. Pierson, C. Rousselot, Stability of reactively sputtered silver oxide films, Surf. Coat. Technol. 200 (2005) 276–279.
[47] J. Pola, S. Bakardjieva, M. Maryško, V. Vorlíček, J. Šubrt, Z. Bastl, A. Galíková, A. Ouchi, Laser-induced conversion of silica into nano-sized carbon–polyoxocarbosilane composites, J. Phys. Chem. C 111 (2007) 16818–16826.
[48] J. Pola, A. Ouchi, S. Bakardjieva, V. Vorlíček, M. Maryško, J. Šubrt, Z. Bastl, Laser photochemical etching of silica: nanodomains of crystalline chaoite and silica in amorphous C/Si/O/N phase, J. Phys. Chem. C 112 (2008) 13281–13286.